International Journal of Heat and Mass Transfer 52 (2009) 5691–5700

Contents lists available at ScienceDirect

International Journal of Heat and Mass Transfer

journal homepage: www.elsevier.com/locate/ijhmt

Experimental and numerical study of heat and moisture transfers by natural convection in a cavity filled with solid obstacles

O. Laguerre [a,*], S. Benamara [a], D. Remy [a], D. Flick [b]

[a] Cemagref, UMR 1145 Génie Industriel Alimentaire, Refrigeration Process Engineering, Cemagref, BP. 44, 92163 Antony Cedex, France
[b] AgroParisTech, UMR 1145 Génie Industriel Alimentaire, AgroParisTech, F-91300 Massy, France

ARTICLE INFO

Article history:
Received 24 November 2008
Received in revised form 18 May 2009
Accepted 10 July 2009
Available online 19 September 2009

Keywords:
Obstacles
Cavity
Natural convection
Radiation
Humidity

ABSTRACT

Heat, moisture transfers and airflow by natural convection in a rectangular cavity containing on line cylinders were studied. The work zone was arranged in such a way that 2D transfer and flow were established. At steady state, temperature, velocity and humidity fields on the symmetry plane were measured in unhumidified and humidified cavity. These results were then used to compare with CFD simulation. The thermal stratification and circular air flow in the cavity was observed. Humidification at the bottom face of cavity contributes to increase air velocity. The influence of radiation near the cold and warm walls is significant.

1. Introduction

Natural convection heat transfer phenomena inside cavities are relevant to a wide range of industrial processes or environmental situations. It has been the subject of a very intense research activity over the past decades and reviews are available: Bejan [1], Khramtsou and Martyneuko [2], Khalifa [3]. The analysis of these studies shows that there are more numerical studies than experimental ones because of difficulties to develop an experimental device with well controlled boundary conditions and instrumentation. These studies concern empty cavities or cavities filled with porous medium but rarely cavities containing numerous obstacles whereas this situation is common in practice. The configuration studied in this work is encountered for example in refrigeration equipments loaded by food products: domestic refrigerator, cheese ripening room, cold room, insulated container, etc. Similar configurations can also be found in other areas, for example greenhouses. The porous media approach is not well adapted in these cases since it is not possible to define correctly a representative elementary volume (small compared to the cavity and containing high number of particles). Moreover, the equivalent properties of the porous medium are difficult to estimate. Thus, a direct Navier Stokes formulation was used for modelling.

1.1. Natural convection in empty cavity

The most studied configuration is a rectangular cavity in which two opposite walls are differentially heated. The 2-dimension case is a classical Benchmark problem (de Vahl Davis [4], Le Queré [5]). The 3-dimension case of a cubical cavity is also used to compare numerical results with experimental ones (Leong et al. [6]). Generally, the Boussinesq approximation is used, but for large temperature difference, this leads to poor accuracy and the low Mach number approximation is preferred (Becker and Braack [7], Weisman et al. [8]).

Experimental fluid flow visualisation (PIV) and temperature measurement in cavity filled by air was carried out by Wu et al. [9]. The influence of wall temperature on laminar airflow ($Ra = 1.3 \times 10^8$) in steady state was studied. Similar study was carried out by Calcagni et al. [10] for $10^3 < Ra < 10^6$, Corvaro and Paroncini [11] for $9.0 \times 10^4 < Ra < 2.7 \times 10^5$, which performed flow visualisation by 2D-PIV and halographic interferometry techniques.

The combined effect of heat and mass transfer was also widely studied (Weaver and Viskanta [12]) notably the case of cavities containing humid air in presence of condensation and evaporation. McBain [13] numerically studied the natural convection in 2D-cavity for different temperatures and humidity on the vertical walls. The simulation takes into account heat and moisture transfer in steady state, laminar regime ($10^4 < Ra < 10^6$) and negligible viscous dissipation. Recently, Debbissi et al. [14,15] numerically investigated the coupled heat and mass transfer by natural or mixed convection during water evaporation in a vertical heated channel.

* Corresponding author. Tel.: +33 1 40 96 61 21; fax: +33 1 40 96 60 75.
E-mail address: onrawee.laguerre@cemagref.fr (O. Laguerre).

0017-9310/$ - see front matter © 2009 Elsevier Ltd. All rights reserved.
doi:10.1016/j.ijheatmasstransfer.2009.07.028

Nomenclature

b	Thickness of boundary layer, m
C_p	Thermal capacity, J kg^{-1} K^{-1}
d	Diameter of the obstacle, m
D	Relative diffusivity of water and air, m^2 s^{-1}
g	Acceleration due to gravity = 9.81 m s^{-2}
h	Heat transfer coefficient, W m^{-2} K^{-1}
H	Height of cavity, m
I	Intensity of radiation, W m^{-2} srd^{-1}
M	Molecular weight, kg mol^{-1}
$\vec{n}$	Normal vector
P	Pressure, Pa
R	Gas constant = 8.31434 J mol^{-1} K^{-1}
T	Temperature, K
t	Time, s
W	Width of cavity, m
x	Mass fraction of water in air kg water/kg humid air
v	Air velocity, m s^{-1}

Greek symbols

λ	Thermal conductivity, W m^{-1} K^{-1}
β	Thermal expansion coefficient, K^{-1}
ρ	Density, kg m^{-3}
ρ_0	Density at reference condition, kg m^{-3}
μ	Viscocity, Pa s
Ω	Solid angle, srd
ϕ	Radiation flux, W m^{-2}
ε_r	Wall emissivity
σ	Boltzmann constant = 5.67 $\times$ 10^{-8} W m^{-2} K^{-4}

Subscripts

amb	Ambient
a	Air
b	Bottom
c	Cold wall
in	Incident
p	Product
o	Reference condition
glob	Global
rad	Radiation
sat	Saturation
t	Top
w	Water

They shown that the evaporative cooling changes the profiles of velocity and temperature considerably especially at the exit of the channel. Hammou et al. [16] have numerically studied the effects of simultaneous heat and mass transfer on downward laminar flow of humid air in a vertical channel with isothermal wet walls. They found that the effects of the buoyancy forces on the hydrodynamic field are very important while their influence on the average air temperature and average mass fraction is small. Yan [17,18] and Fedorov et al. [19] investigated the influences of wetted wall on laminar or turbulent mixed convection heat and mass transfer in vertical channels. The results showed that the effects of the evaporation of water vapour on the heat transfer are rather substantial. Desrayaud and Lauriat [20] studied natural convection of laminar flow of humid air in a vertical channel. They propose correlations for latent and sensible heat transfer. Recently, Laaroussi and Lauriat [21] studied numerically thermosolutal convection and condensation of humid air in cavities with the low Mach number assumption using the finite volume code Fluent.

1.2. Natural convection in cavity filled by solid products

The most studied configuration for natural convection in cavity filled by solid products is that of a porous medium in a rectangular enclosure. The model are based on extended, space averaged, Darcy equations. Most recently, the trend in the research community has shifted to the examination of simultaneous heat and mass transfer or double diffusion convection in enclosures (Gobin et al [22]).

Some studies deal with cavities containing one (Das and Reddy [23]) or several solid objects (Merrikh and Lage. [24], Braga and de Lemos [25,26], Laguerre et al [27]). Merrikh and Lage [24] used the direct CFD approach (Navier Stokes equations) in the case of natural convection within up to 64 solid particles. They studied fluid flow and heat transfer in a differentially heated square enclosure with disconnected solids blocks. Two dimensional laminar simulations were performed for a Prandtl number equal to one, a Rayleigh number ranging from 10^5 to 10^8, a fluid/solid thermal conductivity ratio from 0.1 to 100 and for different numbers (9–64) of solid blocks (constant fraction of volume occupied by the blocks: 36%). They found that when only a few solid blocks were used, the fluid flows predominantly along the channel between the heated (or cooled) wall and the first column of blocks. When more numerous blocks were used, greater fluid flow occurs in some interior channels. This phenomenon is of great importance in terms of wall to fluid heat transfer. Braga and de Lemos [25] studied numerically (direct CFD approach) the laminar natural convection in cavities filled with circular and square rods. They show also that when the number of rods increases, the flow tends to migrate away from the wall due to the increased flow resistance close to the solid wall. Laguerre et al [27] studied experimentally and numerically the laminar natural convection in a cavity containing 180 spheres. They compared the experimental results with direct CFD simulations (Navier Stokes equations) and with porous medium simulations (extended Darcy equations). These two simulations included conduction, convection and radiation. Braga and de Lemos [26] also compared the two modelling approaches and included additional phenomena such as turbulence in further studies.

The present work was carried out to enrich the knowledge on the phenomena which take place in a cavity more or less humidified containing numerous obstacles. The combined effect of heat, mass and momentum transfer was studied. First, the experimental results of temperature, velocity and humidity fields are presented. Then, CFD simulations (direct approach) are compared with the experimental results.

2. Materials and methods

Experimental device and measurement methods will be presented firstly. Then, model hypothesis, initial and boundary conditions used in CFD simulation will be explained.

2.1. Experiment

2.1.1. Experimental device

The experimental device (Fig. 1) is composed of a rectangular cavity (internal dimension 1 m $\times$ 0.5 m $\times$ 0.5 m). One of the vertical walls, made of aluminium, is kept at low temperature. The opposite wall is made of double glass (glass thickness of 6 mm and air thickness between glass walls of 10 mm) and involves heat

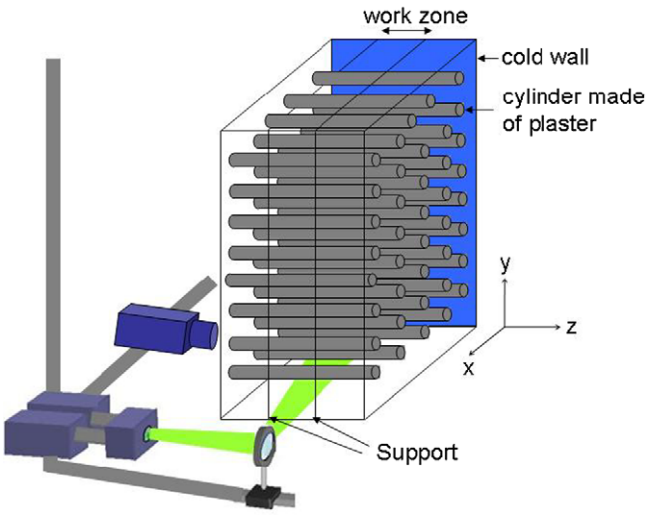

Fig. 1. Experimental device.

transfer with the ambience. A low temperature water-glycol mixture is prepared in a thermostatically controlled cooling bath and circulates through a coil inside the aluminum wall to maintain it at a constant temperature.

The top and bottom horizontal walls are made of PVC (thickness of 2 cm). The side and top walls are insulated using expanded polystyrene plates (thickness of 4 cm). These plates can be partially taken off to visualise airflow in the cavity and to measure air velocity by a PIV system. Oil smoke is used as tracer (particle diameter ~1 μm, manufacturer data). The oil droplet displacement is assumed to represent the air velocity.

The cavity is separated into three zones by polycarbonate plates of 1 cm thickness in order to create 2-dimensional flow in the work zone located at the centre. This zone (16 cm width) is bounded and insulated by the lateral ones. The front vertical wall is not insulated in order to enhance the exchanges with the external ambience. Therefore, the heat transfer in the lateral direction (z) can be neglected compared to the heat flux between the cold wall and the front vertical wall. Thus, 2-dimensional heat transfer and flow is assumed. Fig. 1 also shows the position of camera and laser; both of them are fixed on a 3D displacement system (precision ±0.1 mm). The cavity is loaded by cylinders made of plaster (5 cm diameter, 48 cm length) arranged in five columns and eight rows. To increase the air humidity in the cavity, a vat (dimension $13 \times 46 \times 4$ cm) filled by water is placed at the bottom of the work zone. A power controlled heating resistance is immerged in the water allowing the increase of water temperature, hence the increase of evaporation rate. All experimental devices are located in a test room in which the temperature is controlled at 21 °C.

The cavity is cooled for 24 h to ensure steady state heat transfer in the cavity, then, measurements of air temperature, velocity and humidity are performed. In the case of air velocity measurement by PIV, the oil smoke is introduced in the cavity and it follows progressively the air circulation in the cavity. The flow stabilization of smoke takes ~45 min, then, the measurement can be undertaken.

2.1.2. Air velocity measurement

The air velocity is measured by PIV system on the symmetry plane of the cavity. The PIV system is composed of CCD camera (12 bits double matrices of 1376×1024 pixels) allowing the acquisition of two images successively within a short time interval. The sequence of images taken by the camera is synchronised with the two laser impulsions. An instantaneous air velocity field is obtained by inter-correlation of two successive images of smoke particles present in a strongly enlightened plane. In our case, a good velocity estimation could be obtained with an image dimension (width × height) of 10 cm × 7.4 cm and a time interval of 1 ms. It should be noticed that the time interval of 1 ms between two laser pulses is the optimum. If the time interval is too low, the distance of particle displacement is too short and consequently, the calculation of air velocity may conduct to error. If the time interval is too high, the particles appearing in the first image disappear in the second. The velocity calculation is thus impossible.

Vector calculation is undertaken from interrogate windows of dimension 32×32 pixels with 50% of overlap between windows. Thus, there are 16 pixels (1.2 mm) between 2 calculated vectors in both horizontal and vertical directions. A mean air velocity field is calculated from 40 couples of images.

The camera and the laser are moved by using a displacement system allowing the change of position of measured windows. 63 windows in the case of cavity without water vat and 58 in the case of cavity with presence of water vat are used to establish the air velocity field on the symmetry plane. The polystyrene insulation is partially and shortly removed for PIV measurement of each window.

2.1.3. Temperature measurement

T-type thermocouples (1 mm diameter, precision ±0.2 °C) are used. These thermocouples are previously calibrated at 5 different temperatures (−10 °C, −5 °C, 0 °C, +10 °C and +20 °C). The temperatures of air, cold and warm walls are measured on the symmetry plane. The temperatures of polycarbonate support, top and bottom walls of the working zone are also measured. The position of these thermocouples is shown in Fig. 2: 45 measurement points for air, 20 for walls. This figure also shows the position of cylinders instrumented by two thermocouples: one at the centre, the other near the surface at the bottom face. For the case of experiments in presence of water vat, 3 thermocouples are used to measure the water temperature. These thermocouples are located on the symmetry plane and at three different distances form the cold wall (10 cm, 25 cm and 40 cm).

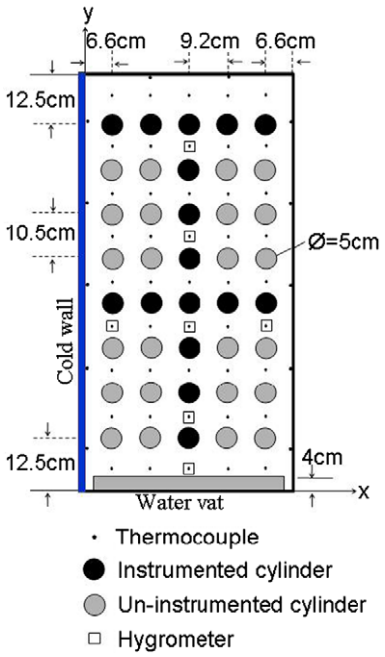

Fig. 2. Side view of work zone showing position of sensors on the symmetry plane.

Precaution is undertaken on the arrangement of thermocouple wires in such a manner that their presence disturbs as less as possible the airflow in the cavity.

2.1.4. Humidity measurement

The air humidity in the cavity is measured at seven positions on the symmetry plane of cavity using hygrometers (Vaisala HMP50, Fig. 2). These sensors are previously calibrated by placing them in an ambient of known relative humidity. In our case, it consists of closed enclosure containing saturated salt (at 20 °C): $Mg(Cl)_2$ (33.1% RH), NaCl (75.5% RH) and $NH_3(SO_4)$ (81.3% RH). These hygrometers are equipped with thermocouples which allow measuring air temperature at the same position. Both measured temperature and relative humidity are used to calculate air density and dew point temperature.

2.1.5. Experimental conditions

In order to avoid the airflow perturbations in the cavity due to the presence of numerous sensors, experiments of air velocity, temperature and humidity measurements were carried out separately. The cold wall of the cavity was maintained at +1 °C during experiment.

The experiment in un-humidified cavity was firstly carried out. Then, humidity in the cavity was increased by the presence of water vat at the bottom of the work zone. This water was maintained at 13.7 °C (13.2 °C near cold wall, 14.1 °C near glass wall) by an immerged regulated heating resistance.

2.2. CFD simulation

Numerical simulation was carried out to predict the combined fluid flow and transfer phenomena in steady state for the un-humidified and humidified cavity. The main hypotheses used are:

- 2-Dimensional airflow, heat and mass transfer (in case of humidification).
- Boussinesq approximation was used in the case of un-humidified cavity to describe air density variation due to temperature. The relative variation of density is less than 5% inside the cavity.
- Perfect gas law was supposed in the case of humidified cavity to describe air density variation due to temperature and humidity (pressure is assumed to be equal to the atmospheric one in this relation).
- Laminar airflow.
- Radiation between surfaces (of cavity or cylinders) was taken into account. These surfaces are supposed to be gray (non-specular). Absorption and diffusion by air is supposed negligible.

2.2.1. For the un-humidified cavity

Assuming the fluid properties to be constant, the flow of incompressible Boussinesq viscous fluid is governed by the following equations:

$$\vec{\nabla}\cdot(\vec{v}) = 0 \tag{1}$$

$$\rho_0\vec{\nabla}\cdot(\vec{v}\otimes\vec{v}) = -\vec{\nabla}p + \mu\vec{\nabla}^2\vec{v} - \rho_0\vec{g}\beta(T-T_0) \tag{2}$$

$$\rho_0 C_p\vec{\nabla}\cdot(T\vec{v}) = \lambda\vec{\nabla}^2 T \tag{3}$$

where ρ_0 is the air density at reference condition.

2.2.2. For the humidified cavity

Conservation of mass, momentum, energy and water leads to the following equations:

$$\vec{\nabla}\cdot(\rho\vec{v}) = 0 \tag{4}$$

$$\vec{\nabla}\cdot(\rho\vec{v}\otimes\vec{v}) = -\vec{\nabla}p + \mu\vec{\nabla}\cdot\left(\vec{\nabla}\cdot\vec{v} + (\vec{\nabla}\cdot\vec{v})^T - \frac{2}{3}(\vec{\nabla}\cdot\vec{v})I\right) + (\rho-\rho_0)\vec{g} \tag{5}$$

$$C_p\vec{\nabla}\cdot(\rho T\vec{v}) = \lambda\vec{\nabla}^2 T \tag{6}$$

$$\vec{\nabla}\cdot(\rho x\vec{v}) = D\vec{\nabla}\cdot(\rho\vec{\nabla}x) \tag{7}$$

An approach similar to the low Mach number approximation was used. The pressure is split into three parts:

$$P = p_0 - \rho_0 gz + p$$

But here p_0 is simply assumed as constant and equal to the atmospheric pressure. Indeed, the experimental device is not a perfectly closed cavity, there is a small opening at the bottom of the cavity which allows the pressure inside the cavity to be equilibrated with the atmospheric pressure (the sensor cables also enters the cavity trough this opening). The air and water fluxes throughout this opening were not modelled because, at steady state, there are equal to zero. The second term represents the hydrostatic part. Only the last term (p) involves fluid motion. At low Mach number, the variation of pressures is small compared to the absolute pressure. Thus, the influence of p and $\rho_0 gz$ can be neglected in the thermodynamic state equation giving density:

$$\rho = \frac{p_0 M_a}{RT}\frac{1}{1+\left(\frac{M_a}{M_w}-1\right)x} \tag{8}$$

This approach avoids the numerical problem related to acoustic waves.

2.2.3. For both un-humidified and humidified cavity

The general equation of heat transfer by radiation (in a given $\vec{s}$ direction) is:

$$\vec{\nabla}\cdot(I(\vec{r},\vec{s})\vec{s}) = 0 \tag{9}$$

where $I(\vec{r},\vec{s})$ is the radiative intensity in $\vec{s}$ direction (at $\vec{r}$ position) (W m^{-2} per unit solid angle).

The general equation of heat transfer by conduction inside the cylinders is:

$$\vec{\nabla}^2 T_p = 0 \tag{10}$$

2.2.4. Boundary conditions

No slip condition applies for all the solid surfaces (cavity wall and surface of cylinders).

The cold wall is assumed as isothermal: $T = T_c$.

In the case of humidified cavity, condensation occurs on the cold wall. The water mass fraction is that of saturation: $x = x_{sat}(T_c)$.

The bottom of cavity, where located the water vat, is also assumed as isothermal: $T = T_b$ (measured mean value).

As evaporation occurs on the water vat, saturation is assumed at this position: $x = x_{sat}(T_b)$.

The other surfaces are assumed to involve neither condensation nor evaporation: $\vec{\nabla}x\cdot\vec{n} = 0$.

For the top wall, the experimental temperature was imposed: $T = T_t$.

At the surface of the cylinders, thermal boundary condition is:

$$-\lambda\vec{\nabla}T\cdot\vec{n} + \phi_{net.rad} = -\lambda_p\vec{\nabla}T_p\cdot\vec{n}$$

$$\text{where}\quad \phi_{net.rad} = \phi_{in} - \phi_{out},\quad \phi_{in} = \int_{\vec{s}\cdot\vec{n}>0} I_{in}\cdot\vec{s}\cdot\vec{n}\cdot d\Omega$$

$$\phi_{out} = (1-\varepsilon_r)\cdot\phi_{in} + \varepsilon_r\sigma T_p^4 \tag{11}$$

The walls are assumed as gray diffuse: $I_{out} = \phi_{out}/\pi$.

Remark, it is theoretically possible that the temperature of a cylinder is lower than the dew point temperature of adjacent air so that condensation would occur on it, this case is not taken into account in the present study.

For the double glass wall, a global heat transfer coefficient (h_{glob}) was estimated taking into account conduction through the glass and the air layer and radiation between the glass walls:

$$-\lambda\vec{\nabla}T\cdot\vec{n}+\phi_{net.rad}=h_{glob}(T-T_{amb}) \quad (12)$$

The equations were solved using the finite volume method (Fluent 6) by using a sequential solver. The radiation equation was discretised using the discrete ordinate method. Firstly, the equations were solved in an unsteady state formulation. This is to avoid a rapid divergence when trying to solve directly the steady state problem with a zero velocity field as the first estimation. When the unsteady state solution began to stabilize, the steady state solver was then used (the velocity field obtained by the unsteady solver was taken as the first estimation). Table 1 summarizes the solver parameters. The mesh is finer near the walls and surface of the cylinders. Table 2 presents physical properties of air and other used material. Table 3 presents boundary conditions parameters.

The influence of meshing and angle discretisation (in radiation equation) on the results was studied in the case of un-humidified cavity. Three number of meshes: coarse (13,354), fine (56,960), extra fine (96,204) and 4 angle discretisation: 2, 4, 16, 24 were used.

3. Results and discussion

3.1. Experimental results

First of all, the experimental results of airflow, temperature and humidity on the symmetry plane are presented. Then, a comparison between the experimental results and those obtained from CFD simulation is shown. It is to be reminded that experiment is carried out at steady state.

3.1.1. Velocity field

For un-humidified cavity, Fig. 3 shows the mean velocity field on the symmetry plane obtained from 40 pairs of images. The vectors are coloured by the velocity magnitude. It can be observed the absence of vector at the bottom of the cavity (from 0 to 2 cm high). This is due to the presence of a support for the polycarbonate separation plates (made of black paint metal) that makes the measurement by PIV impossible. It can also be observed the absence of vector between two cylinders due to the lack of laser sheet in this zone. On this figure, values of air density (kg/m^3) at certain positions are also indicated. These values are calculated from the measured air temperature and relative humidity at that position. The air density decreases from the bottom (1.243 kg/m^3) to the top (1.227 kg/m^3), this reflects the stratification effect. Density also decreases from the cold wall (1.243 kg/m^3) to the warm wall (1.234 kg/m^3), this density difference is the driving force of air motion whereas friction with the walls and the cylinders limit air circulation. It can be noticed that the maximum (measured) density difference is 1.243−1.227 = 0.016 kg/m^3. Taking a characteristic height of 1 m, this represents a gravitational volumic energy of about 0.16 J/m^3, in other words, an equivalent driving pressure difference of 0.16 Pa.

Circular airflow is observed: air flows downward near cold wall and upward near warm wall. Near the cold wall, air velocity increases progressively from the top to attain the maximum value at the bottom (0.25 m/s). Near the warm wall, air velocity is nearly constant from the bottom to the top. This is due to the difference of boundary conditions near the cold wall (Dirichlet condition, T = 1 °C) and near the opposite wall (Cauchy condition, h_{glob} = 7 W m^{-2} °C^{-1}, T_{amb} = 21 °C). This main circular airflow occurs very near to the wall. The thickness of the hydrodynamic boundary layer is typically of 2 cm. The cylinders do not interact directly with this circular air flow. Moreover, air flows horizontally from warm wall to join the cold wall in the upper part of the cavity. This flow is wavy and the velocity is about 0.05 m/s above the 6th row of cylinder. In the lower part of the cavity, air velocity between cylinders is very low (<0.02 m/s). It can also be observed the downward airflow around the column of cylinders located the nearest to cold wall and upward airflow around the column the nearest to warm wall.

For humidified cavity, the mean air velocity on the symmetry plane of and the air density of certain positions are similar to those of un-humidified cavity. The density decreases from the bottom to the top and from the cold wall to the warm wall. Circular airflow near the walls is also observed. But, the maximum velocity magnitude observed near the cold wall is higher (0.275 m/s instead of 0.25 m/s). The velocity near the warm vertical wall is also higher. Generally, velocity magnitude is higher whatever the position in the cavity. This is mainly due to the combined effect of temperature and humidity variation. Indeed, on one hand, the heated water vat increases temperature and water content of the air just over it, which leads to decrease air density. On the other hand, temperature decreases and water vapour condenses on the cold wall, which leads to increase density. Cold and rather dry air (high density) comes down from the cold wall to the left bottom corner and flows toward the right corner. This air is heated and humidified (becoming lower density) by the water vat and then flows upwards along the warm wall.

3.1.2. Temperature field

Air, cylinder and cavity wall temperatures were measured in steady state. The interpolated temperature field established for un-humidified cavity is shown in Fig. 4. The values indicated on the circles represent the average temperature of surface and centre of cylinders and the ones indicated on air field represent the air temperature. It is to be noted that at steady state, the centre temperature of cylinders is very close to that of the surface (difference $\leqslant$ 0.3 °C), except for the two cylinders located near the cold wall at the 4th row from the bottom (difference $\sim$ 0.5 °C). This

Table 1
Solver parameters.

	Under-relaxation coefficient	Type of discretisation
Pressure	0.8	Presto
Density	1	–
Gravity forces	1	–
Momentum	0.2	Second order upwind
Energy	0.6	Second order upwind
Water vapor	1	Second order upwind
Radiation	0.5	–
Pressure-velocity	–	Simple

Table 2
Physical properties of materials involved in simulations.

Air (at 2 °C)	Value	Unit
Density	1.278	kg m^{-3}
Thermal capacity	1006	J kg^{-1} K^{-1}
Viscosity	17.21×10^{-6}	Pa s
Thermal conductivity	24.3×10^{-3}	W m^{-1} K^{-1}
Coefficient of thermal expansion	3.636×10^{-3}	K^{-1}
Plaster		
Thermal conductivity	0.35	W m^{-1} K^{-1}
Glass		
Thermal conductivity	0.75	W m^{-1} K^{-1}

Table 3
Boundary conditions parameters.

Material	Cold wall Aluminum Imposed temperature			Top horizontal wall PVC + extruded polystyrene Imposed temperature			Bottom horizontal wall PVC + extruded polystyrene Imposed temperature			Side wall Glass Transfer coefficient + ambient temperature		
Boundary condition	T_{wall} (°C)	ε_r	x_{H_2O}[d]	T_{wall}	ε_r	–	T_{wall} (°C)	ε_r	x_{H_2O}	h_{glob}	T_{amb} (°C)	ε_r
Un-humidified cavity	1.1	0.90[a]	–	14.1	0.90[b]	–	8.8	0.90	–	7	21	0.90[c]
Humidified cavity	1.2	0.90	4.07	14.4	0.90	–	13.7	0.90	9.68	7	21	0.90

[a] Dow [30].
[b] Wen and Mudawar [31].
[c] Pieters et al. [32].
[d] Unit (g water/kg dry air).

figure shows that the cylinder and air temperatures increase with the height. This stratification effect (cold air is heavier than warm air) is in agreement with the velocity field presented previously: downward airflow near the cold wall and upward airflow near the warm wall. At the same height, the cylinder temperature also increases from the cold wall side to the warm wall side. Obviously, air temperature also increases from cold wall maintained at 1 °C to the warm wall whose temperature increases linearly from 11 °C near the bottom to 17 °C near the top.

It can be observed that near the cold wall, the average cylinder temperature is slightly lower than the surrounding air temperature. This difference is due to radiation. Indeed, at steady state and without radiation, the cylinder temperature should be the same as the one of surrounding air. In our experiment, heat exchange by radiation between the cold wall and product surface contributes to cool down the product. In the same manner, heat exchange by radiation between the warm wall and product surface leads to increase the product temperature. In our case, radiation

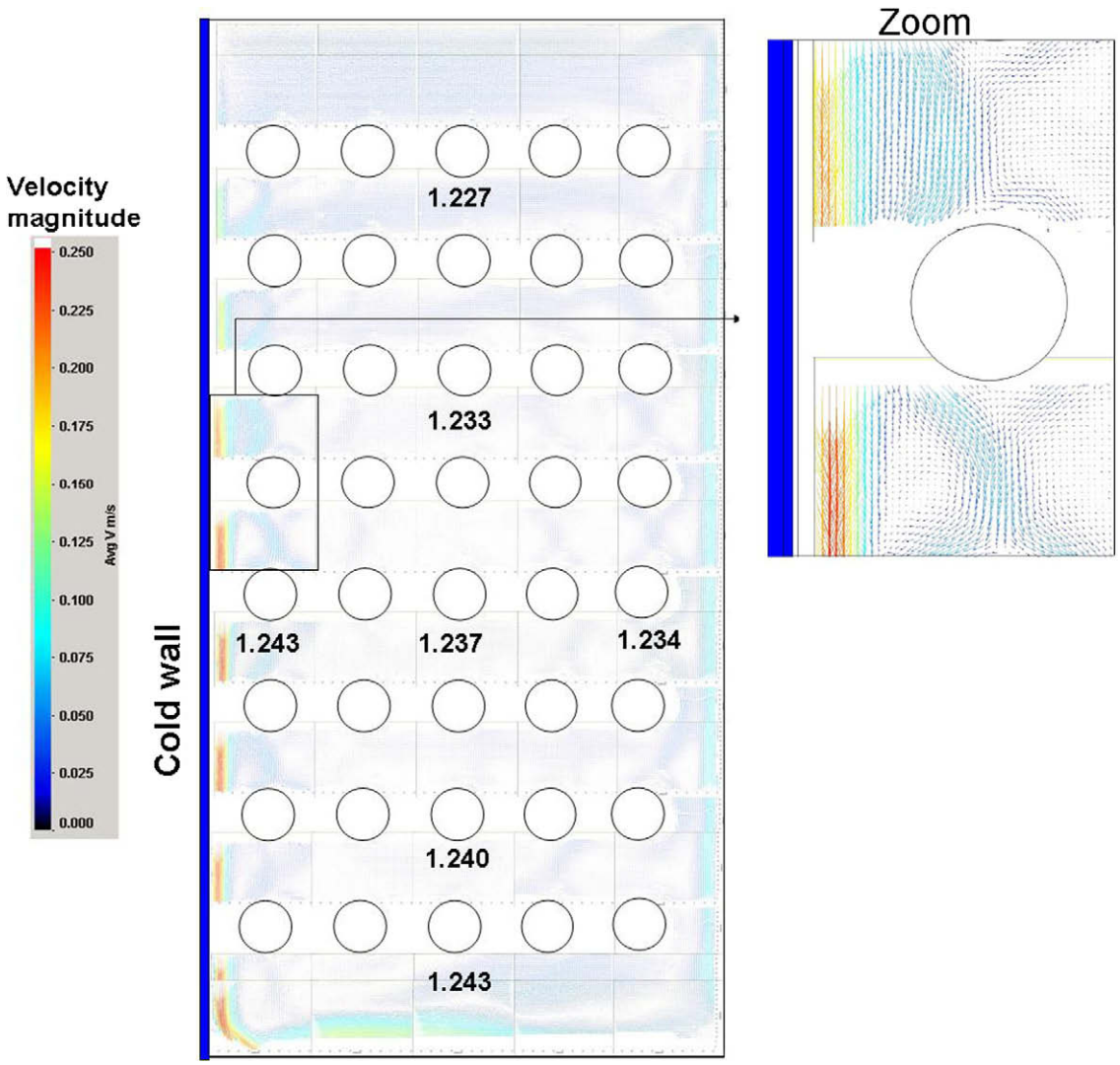

Fig. 3. Mean air velocity field on the symmetry plane of un-humidified refrigerating cavity (cold wall maintained at 1 °C, ambience at 21 °C), values represent air density (kg m^{-3}) calculated from measured temperature and humidity.

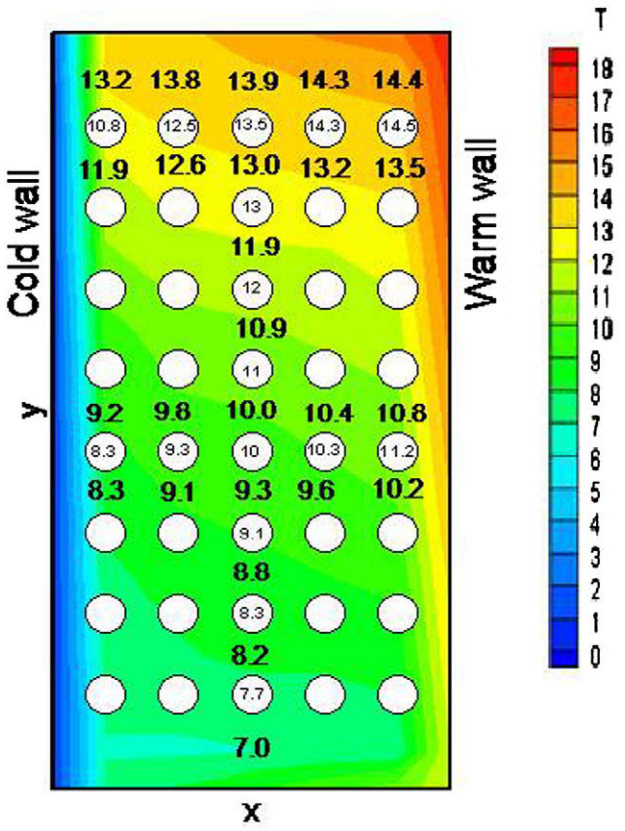

Fig. 4. Temperature field on the symmetry plane of un-humidified refrigerating cavity (cold wall maintained at 1 °C). Value in circle represents average cylinder temperature (°C) and the one around certain cylinders represent air temperature (°C).

is not negligible compared to convection so that a cylinder located near the wall is at intermediate temperature between the surrounding air, with which it exchanges heat by convection and the wall, with which it exchanges heat by radiation. In addition to the primary natural convection flow near the walls due to temperature difference between the vertical walls and the adjacent air, a secondary natural convection flow around the cylinders is due to the temperature difference between the cylinders and the surrounding air. This is in agreement with velocity measurements. For example, at mid-height near the cold wall, product temperature is less than the one of air because of radiation between cold wall and product surface. This temperature difference induces natural convection effect which can be observed in Fig. 3.

For humidified cavity, temperature stratification similar to that of the un-humidified cavity was obtained. Due to radiation, the temperature of the cylinders is still lower than the surrounding air near the cold wall and this temperature is higher than that of surrounding air near the warm wall. The presence of the heated water vat (at 13.7 °C) leads to more pronounced temperature elevation at the bottom than at the top.

3.1.3. Humidity field

For humidified cavity, the relative humidity decreases with the height and with the distance from cold wall. The value varies from 82% at the bottom to 70% at the top and it varies from 90% near the cold wall to 76% near the warm wall. This trend can be explained by the fact that at the water vat surface where evaporation occurs and at the cold wall where condensation occurs, relative humidity is, a priori, 100% (saturation). On the other hand, relative humidity decreases because temperature increases without change of water content near the warm wall.

3.2. Numerical results and comparison with experimental values

3.2.1. Sensitivity study

Three different mesh fineness and four angle discretisation were used in this study. A comparison of temperature profile on the central axis of the un-humidified cavity was undertaken. It was observed that the difference is not significant between the results of fine and extra fine mesh and between 4, 16 and 24 discrete angle. Using the coarse mesh or only two discrete angles leads to very different results compared to the others. A comparison of velocity profile was also undertaken and it leads to the same conclusion. Therefore, the fine mesh and 4 discrete angles were used for the simulations both in un-humidified and humidified cavities. A comparison between the experimental and numerical results is presented below. Simulation was carried out with and without radiation in order to evaluate the importance of this heat transfer mode.

3.2.2. Comparison between experimental and numerical results

A comparison between the experimental and numerical results was undertaken in the case of un-humidified and humidified cavities. For both cases, the same trend was observed, thus, only the results of humidified cavity are shown.

The vertical temperature profile near the cold wall in humidified cavity is presented in Fig. 5. Temperature stratification is predicted (low temperature at the bottom and high temperature at the top) in presence or absence of radiation. However, when radiation is not taken into account, air temperature is under predicted at the bottom and over predicted at the top of the cavity. When radiation is taken into account (with emissivity of 0.9), the oscillations in the predicted profile can be explained by the fact that air temperature is higher than that of product. This was observed experimentally and related to the radiation between the cold wall and the first column of cylinders. But the temperature difference observed experimentally between cylinders and surrounding air is lower than the predicted one.

Globally, simulation with radiation leads to better agreement with the experimental results. Nevertheless, it seems that the effect of radiation is over-estimated. This could be due to the fact that, like the other phenomena, radiation is assumed as 2D whereas 3D radiation effects occur in reality. Radiation between the cold wall and a cylinder (a in Fig. 6) and between two cylinders (b) is taken into account in 2D simulation. The later phenomena tends to enhance transfer between the top and the bottom parts of cavity and to reduce temperature heterogeneity. But, radiation

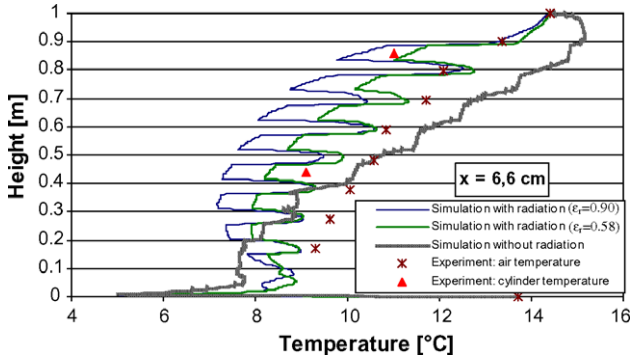

Fig. 5. Comparison between experimental and simulated vertical temperature profile near cold wall (x = 6.6 cm) in humidified cavity (water vat at 13.7 °C).

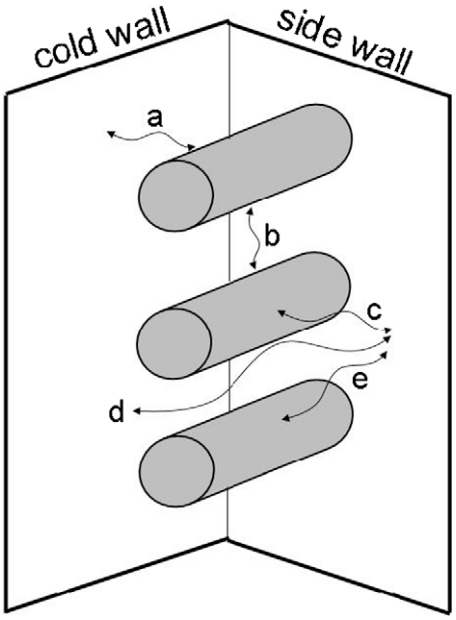

Fig. 6. Radiation inside working zone.

from a cylinder to lateral polycarbonate separation plate (c), which in turn radiates on the cold wall (d) or on another cylinder (e), is not taken into account. In other words, in the experimental configuration, an infrared ray often encounters the lateral wall before "re-emission". This is like a radiation shield effect. To avoid the complexity of the studied geometry, and as a first approach, it was assumed that this 3D radiation shield effect can be taken into account like for radiation between parallel plates with one shield. The emissivity of the walls and of the cylinders is 0.9. The radiation flux between two plates of emissivity ε_1 and ε_3 when a thin shield of emissivity ε_2 is placed between them is:

$$\phi_{\text{rad}} = \frac{A\sigma(T_1^4 - T_3^4)}{\left(\frac{1}{\varepsilon_1} + \frac{1}{\varepsilon_2} - 1\right) + \left(\frac{1}{\varepsilon_2} + \frac{1}{\varepsilon_3} - 1\right)} \tag{13}$$

If $\varepsilon_1 = \varepsilon_2 = \varepsilon_3 = 0.9$, this radiation flux can be rewritten

$$\phi_{\text{rad}} = \frac{A\sigma(T_1^4 - T_3^4)}{\left(\frac{1}{\varepsilon_{\text{eq}}} + \frac{1}{\varepsilon_{\text{eq}}} - 1\right)} \tag{14}$$

where $\varepsilon_{\text{eq}} = 0.58$ is an equivalent emissivity which is lower than that of the surface materials. It allows taking approximately into account the 3D radiation effects in 2D simulations.

This effect could be minimized by using separation plates of low emissivity (made of metal) but this would not allow PIV measurement. Therefore, it is proposed to take into account of 3D radiation effect by using a reduced equivalent emissivity. Fig. 5 shows simulation with an equivalent emissivity of 0.58 which seems in better agreement with experimental results (temperature difference < 1.5 °C).

The comparison between experimental and simulated results near the warm wall confirms the importance of radiation (results are not presented here). It was observed that the effect of radiation is less noticeable at the central axis ($x = 25$ cm) compared to those near the cavity walls.

Horizontal profiles at the mid-height of the cavity for air temperature (Fig. 7) and velocity (Fig. 8) are also compared to the experimental ones. The decay in temperature profile could be due to 3D effects, notably for radiation as discussed before. As the Reyleigh number is relatively high ($\text{Ra} \approx 10^9$), the 2D flow

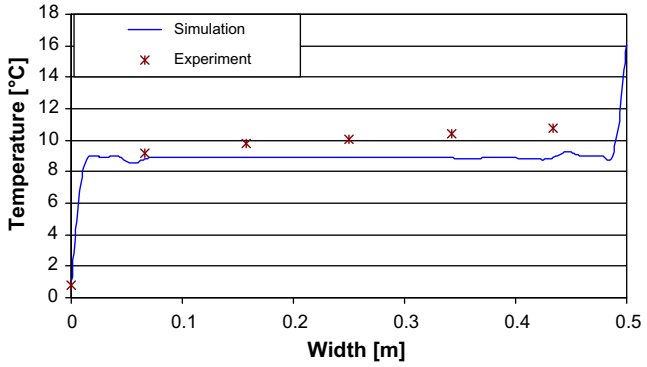

Fig. 7. Comparison between experimental and numerical air temperature profiles (with radiation, $\varepsilon = 0.58$) at mid-height ($y = 49$ cm) of humidified cavity (water vat at 13.7 °C).

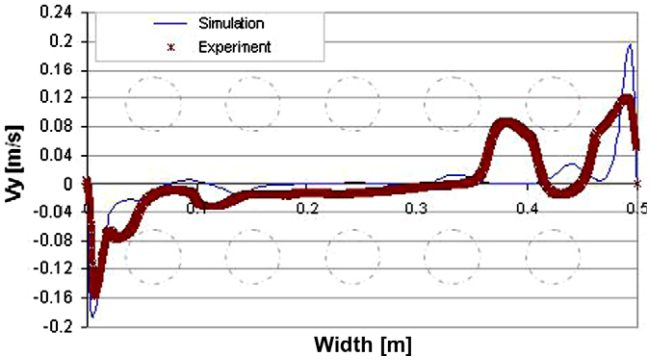

Fig. 8. Comparison between experimental and numerical air velocity profiles (with radiation, $\varepsilon = 0.58$) at mid-height ($y = 49$ cm) of humidified cavity (water vat at 13.7 °C).

could also be instable to 3D disturbances (Penot et al. [28]). It can be observed that near the first column of cylinders near the cold wall (respectively last), the temperature becomes locally lower (respectively higher). This corresponds to specific path lines around the cylinders which are related to local increase of velocity. The predicted velocity is close to the experimental one except in the boundary layer near the warm wall. At this position, the simulation over-estimates the experimental value. This may be due to the over-estimation of the global heat transfer coefficient on the warm wall which leads to an overestimation of warm wall temperature and thus, of the air velocity near this wall. It can also be due to vertical heat transfer, notably by conduction, inside the double glass warm wall which is not taken into account in the simulation.

A great difference of velocity profile is observed between two cylinders near the warm wall. This reflects a difference of local flow pattern. The experimental results show that the upward flow is separated into two streams of about same importance, whereas the numerical results show that the upward flow is mainly near the wall with two others secondary streams. The flow pattern depends on boundary layer separation phenomena and Coanda attachment phenomena which are difficult to predict precisely and which have sometimes a random aspect (Wallis [29]).

Fig. 9 shows a comparison of vertical profile of the experimental and numerical relative humidity in the humidified cavity. The simulation slightly over-predicts the experimental value (maximum difference 5%). An analysis of the numerical result shows that the dew point temperature of surrounding air is higher than that of cylinders surface. In fact, the relative humidity of air around the cylinders is always less than 98%. Thus, the assumption of no

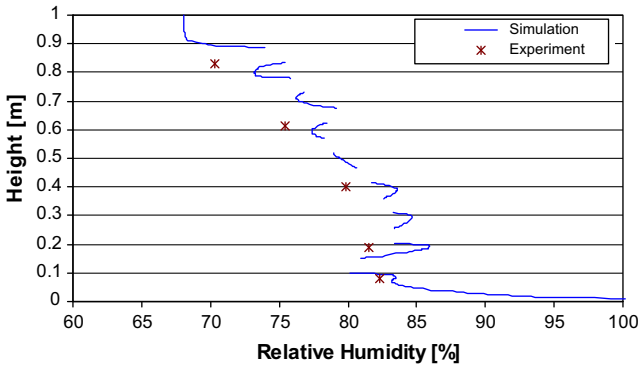

Fig. 9. Comparison between experimental and numerical air relative humidity (with radiation, $\varepsilon = 0.58$) on the central axis ($x = 25$ cm) of humidified cavity (water vat at 13.7 °C).

condensation on the cylinders is applicable here. The calculated evaporation mass flow rate is 5.5×10^{-6} kg/s (for a cavity of 1 m in depth).

Despite of its approximation, the model can predict the general trends (general flow pattern, thickness of the boundary layers, etc.) and some typical parameters (temperature of the obstacles near the cold and the warm wall, temperature and relative humidity variation versus height position, etc.) if some precaution are taken (mesh sensitivity, surface radiation). But it is not able to predict in detail the local flow, temperature and humidity fields.

4. Conclusions

Free convection was studied inside a rectangular cavity ($H/W = 2$) containing obstacles typically 10 times smaller than the cavity ($d/W = 1/10$). These obstacles were evenly distributed in the cavity and occupied about 15% of the cavity volume. This cavity was filled with un-humidified and humidified air and the Rayleigh number was about 10^9. The experiment was performed in a rectangular cavity equipped with one vertical cold wall (made of aluminium) whereas the opposite vertical wall (made of double glass) involved heat exchanges with the ambiance.

Air velocity, temperature and humidity fields on the symmetry plane were measured by PIV, thermocouple and hygrometer respectively. The influence of humidification introduced at the bottom of cavity was studied and compared with the case of un-humidified cavity. The presence of water evaporation and condensation leads to increase air velocity whatever the positions in the cavity. In both cases (un-humidified and humidified cavity) near the cold wall (respectively warm wall) the temperature of the cylinder is lower (respectively higher) than that of surrounding air. This observation demonstrates the importance of radiation between cylinder and cavity walls.

The experimental results were compared to those obtained from CFD simulation for laminar flow in steady state. Boussinesq approximation was used for un-humidified cavity and perfect gas law for humidified cavity. The general trends, experimentally observed, are well predicted notably thermal stratification and difference between cylinder and surrounding air temperature when radiation is taken into account. Nevertheless, some differences appear between experimental and numerical results. This may be partly due to phenomena not taken into account in the model (3D radiation, vertical transfer inside the warm wall). These phenomena are difficult to minimize because of the optical air flow measurement. The differences may be also partly due to the difficulty to predict precisely position of separation and attachment of flow stream in presence of numerous obstacles.

Some general conclusions are presented below:

- The main circular air flow near the cavity walls occurs in a boundary layer which thickness b is small compared to cavity dimension (typically $b/W \approx 0.05$) and even compared to the obstacle ($b/d \approx 0.5$) so that the obstacles interact slightly with this hydrodynamic boundary layer.
- For obstacles and walls of emissivity close to 1, radiation (between two obstacles or between an obstacle and a wall) can not be neglected for the estimation of the temperature field.
- The radiation between a wall and the layer of obstacles close to it explains that the temperature of an obstacle is higher (near a warm wall) or lower (near a cold wall) than the temperature of surrounding air.
- The radiation between the obstacles located at the top of the cavity and those located at the bottom (combined with the convective exchanges between the obstacles and the air) reduces thermal stratification (temperature difference between top and bottom of the cavity is lower in presence of radiation).

The methodology developed in this work can be applied, for example, to the case of loaded refrigerating equipments, in order to better control product quality.

Acknowledgements

The authors would like to thank the French National Research Agency for the financial support, D. Gobin and S. Mergui (Laboratoire Fast, Campus Universitaire, 91405 Orsay, France) for their scientific suggestions.

References

[1] A. Bejan, Convection Heat Transfer, third ed., Wiley, New York, 2005.
[2] P.P. Khramtsou, O.G. Martyneuko, Free Convection Heat transfer, Springer Edition, 2005.
[3] A.J. Khalifa, Natural convection heat transfer coefficient – a review II. Surface in two- and three-dimensional enclosures, Energy Conversion and Management 42 (2001) 505–517.
[4] G. de Vahl Davis, Natural convection of air in a square cavity: a benchmark numerical solution, Int. J. Num. Methods Fluids 3 (1983) 249–264.
[5] P. Le Queré, Accurate solutions to the square thermally driven cavity at high Rayleigh number, Comput. Fluids 20 (2001) 29–41.
[6] W.H. Leong, K.G.T. Hollands, A.P. Brunger, Experimental Nusselt numbers for a cubical-cavity benchmark problem in natural convection, Int. J. Heat Mass Transfer 42 (1999) 1979–1989.
[7] R. Becker, M. Braack, Solution of a stationary benchmark problem for natural convection with large temperature difference, Int. J. Therm. Sci. 41 (2002) 428–439.
[8] C. Weisman, L. Calsyn, C. Dubois, P. Le Quéré, Sur la nature de la transition à l'instationnaire d'un écoulement de convection naturelle en cavité différentiellement chauffée à grands écarts de température, CR. Acad. Sci. Paris t.329 (Série IIb) (2001) 343–350.
[9] W. Wu, D. Ewing, C.Y. Ching, The effect of the top and bottom wall temperature on the laminar natural convection in an air-filled square cavity, Int. J. Heat Mass Transfer 49 (2006) 1999–2008.
[10] B. Calcagni, F. Marsili, M. Paroncini, Natural convective heat transfer in square enclosures heated from below, Appl. Therm. Eng. 25 (2005) 2522–2531.
[11] F. Corvaro, M. Paroncini, Experimental analysis of natural convection in square cavities heated from below with 2D-PIV and halographic interferometry techniques, Exp. Therm. Fluid Sci. 31 (2007) 721–739.
[12] J.A. Weaver, R. Viskanta, Natural convection due to horizontal temperature and concentration gradients. 1. Variable thermophysical properties effects, Int. J. Heat Mass Transfer 34 (1991) 3107–3120.
[13] G.D. McBain, Natural convection with unsaturated humid air, Int. J. Heat Mass Transfer 40 (1997) 3005–3012.
[14] C. Debbissi, J. Orfi, S. Ben Nasrallah, Evaporation of water by free convection in a vertical channel including effects of wall radiative properties, Int. J. Heat Mass Transfer 44 (2001) 811–826.
[15] C. Debbissi, J. Orfi, S. Ben Nasrallah, Evaporation of water by free or mixed convection into humid air and superheated steam, Int. J. Heat Mass Transfer 46 (2003) 4703–4715.

[16] Z.A. Hammou, B. Benhamou, N. Galanis, J. Orfi, Laminar mixed convection of humid air in a vertical channel with evaporation or condensation at the wall, Int. J. Therm. Sci. 43 (2004) 531–539.
[17] W.M. Yan, Mixed convection heat transfer enhancement through latent heat transport in vertical parallel plate channel flows, Can J. Chem. Eng. 69 (1991) 1277–1282.
[18] W.M. Yan, Turbulent mixed convection heat and mass transfer in a wetted channel, ASME J. Heat Transfer 117 (1995) 229–233.
[19] A.G. Fedorov, R. Viskanta, A.A. Mohamad, Turbulent heat and mass transfer in an asymmetrically heated, vertical parallel-plate channel, Int. J. Heat Fluid Flow 18 (1997) 307–315.
[20] G. Desrayaud, G. Lauriat, Heat and mass transfer analogy for condensation of humid air in a vertical channel, Heat Mass Transfer 37 (2001) 67–76.
[21] N. Laaroussi, G. Lauriat, Conjugate thermosolutal convection and condensation of humid air in cavities, Int. J. Therm. Sci. 47 (2008) 1571–1586.
[22] D. Gobin, B. Goyeau, A. Neculae, Convective heat and solute transfer in partially porous cavities, Int. J. Heat Mass transfer 48 (2005) 1898–1908.
[23] M.K. Das, S.K. Reddy, Conjugate natural convection heat transfer in a inclined square cavity containing a conducting block, Int. J. Heat Mass Transfer 49 (2006) 4987–5000.
[24] A.A. Merrikh, J.L. Lage, Natural convection in an enclosure with disconnected and conducting solid blocks, Int. J. Heat Mass Transfer 48 (2005) 1361–1372.
[25] E.J. Bragas, M.J.S. de Lemos, Laminar natural convection in cavities filled with circular and square rods, Int. Commun. Heat Mass Transfer 32 (2005) 1289–1297.
[26] E.J. Bragas, M.J.S. de Lemos, Heat transfer in enclosures having a fixed amount of solid material simulated with heterogeneous and homogeneous models, Int. J. Heat Mass Transfer 48 (2005) 4748–4765.
[27] O. Laguerre, S. Ben Amara, G. Alvarez, D. Flick, Transient heat transfer by free convection in a packed bed of spheres: comparison between tow modelling approaches and experimental results, Appl. Therm. Eng. 28 (2008) 14–24.
[28] F. Penot, M. Dame, P. Le Queré, Investigation of the route to turbulence in a vertical differentially heated cavity, in: Proceeding of the ninth international Heat Transfer Conference, 2, Jerusalem, 1990, pp. 417–422.
[29] R.P. Wallis, Photographic study of fluid flow between banks of tubes, Engineering 148 (1939) 423–425.
[30] DOW, Propriétés Spécifiques des Panneaux Isolants, Programme STYROFOAM: L'isolation des Spécialistes, Editions ROULAND, Paris, 1991.
[31] C.D. Wen, I. Mudawar, Emissivity characteristics of roughened aluminum alloy surfaces and assessment of multispectral radiation thermometry (MRT) emissivity models, Int. J. Heat Mass Transfer 47 (2004) 3591–3605.
[32] J.G. Pieters, J.M.J.J. Deltour, M.J.G. Debruyckere, Onset of condensation on the inner and outer surface of greenhouse covers during night, J. Agric. Eng. Res. 61 (1995) 165–171.